

High-Power 1.5- μm Broad Area Laser Diodes Wavelength Stabilized by Surface Gratings

Antti T. Aho^{ID}, Jukka Viheriälä^{ID}, Heikki Virtanen^{ID}, Topi Uusitalo^{ID}, and Mircea Guina^{ID}

Abstract—Wavelength stabilization against temperature variation of high-power broad area 1.5- μm InGaAsP/InP laser diodes is demonstrated by employing surface gratings. The development targets application in eye-safe automotive LIDAR systems, which would benefit from deploying narrowband receiver filters to block ambient solar radiation for improved signal-to-noise ratio. The surface grating is monolithically integrated on the laser chip using nanoimprint lithography. The peak power of the lasers exceeded 6 W in pulsed mode, for an FWHM spectral width of 0.3 nm and a peak wavelength drift of only 0.1 nm/ $^{\circ}\text{C}$. The wavelength shift with temperature is reduced by five times compared to broad area high-power Fabry–Perot laser diodes typically employed in LIDAR systems.

Index Terms—Diode lasers, distributed Bragg reflector, high power, LIDAR.

I. INTRODUCTION

LIDAR applications are experiencing a fast rate of development owing to many high-value emerging needs, such as obstacle detection and avoidance for autonomous vehicles, robotics, and augmented reality. To this end, the 800 nm–900 nm wavelength range is commonly used since both high-power laser sources and low noise cheap and fast detectors are readily available [1]. However, a serious limitation in this wavelength range is the requirement for eye-safety, which limits the maximum permissible output power and thus the range of the LIDAR imaging. A higher output power can be used at longer wavelengths: for example, the maximum permissible exposure (MPE) of the human cornea for a 1 μs laser pulse is 1 Jcm^{-2} at 1500 nm but only 32×10^{-7} Jcm^{-2} at 800 nm [2]. Additional benefits obtained by using longer wavelengths are reduced scattering by small particles, which enhances the operation capability in adverse weather conditions [3], and a low level of optical losses caused by the atmosphere, both limiting the visibility range of the LIDAR systems working at shorter wavelengths.

The wavelengths around 1.5 μm are commonly used in military LIDAR and range-finding applications [4], but since

Manuscript received August 24, 2018; accepted September 11, 2018. Date of publication September 17, 2018; date of current version November 6, 2018. This work was supported in part by the H2020-ECSEL-2015 Project DENSE under Grant 692449, in part by the HPY Research Foundation, in part by the Finnish Foundation for Technology Promotion, in part by the KAUTÉ Foundation, and in part by Emil Aaltonen's Foundation. (*Corresponding author: Antti T. Aho*)

The authors are with the Optoelectronic Research Centre, Tampere University of Technology, 33720 Tampere, Finland (e-mail: antti.t.aho@tut.fi; jukka.viheriala@tut.fi; heikki.a.virtanen@tut.fi; topi.uusitalo@tut.fi; mircea.guina@tut.fi).

Color versions of one or more of the figures in this letter are available online at <http://ieeexplore.ieee.org>.

Digital Object Identifier 10.1109/LPT.2018.2870304

they are often based on a fiber laser [5], many current solutions are too bulky and unwieldy for compact applications. Since the output power of 1.5 μm diode lasers is lacking compared to 1.5 μm fiber lasers and 900 nm diode lasers, a precisely controlled narrow spectrum is advantageous in sensing applications because it enables the use of narrow passband optical filters in front of the sensor, reducing the solar background noise and improving the signal-to-noise ratio.

To address these application challenges, we demonstrate a 1.5 μm broad area laser diode with a monolithically integrated Bragg grating to act as a compact, cost-effective high-power laser source at an eye-safe wavelength and exhibiting a well-controlled and narrow spectrum. Recently, broad area distributed Bragg reflector laser diodes (DBR-LDs) have been demonstrated at 905 nm with 50 W output power in 10 ns pulsed operation [6]. Moreover, a broad area distributed feedback (DFB) laser has been demonstrated, exhibiting 5.5 W output power around 970 nm [7]. At 1.55 μm , a high-power DBR-LD has been demonstrated using a tapered power amplification section resulting in 0.6 W CW power [8], while we demonstrated pulsed operation from a similar kind of component with 1.6 W peak power [9].

We incidentally show that the wavelength locking with a DBR geometry eliminates the wavelength variation caused by the change in the gain spectrum over the semiconductor substrate, which typically causes a variation of emission spectrum in broad area Fabry-Perot (FP) high-power lasers, reducing the yield of components emitting at a specific peak wavelength. The gratings also provide wavelength stability against temperature variation, resulting in a wavelength drift reduced by about five times compared to the FP-LD, again enabling the use of narrow band-pass receiver filters. We elaborate the fabrication of the DBR-LD based on regrowth-free surface gratings patterned with soft-UV Nanoimprint Lithography (NIL) – a combination enabling cost-effective grating fabrication. Additionally, monolithically integrated gratings avoid the need to precisely assemble and adjust the external grating elements one-by-one as is the case with, for example, volume Bragg grating technology. Finally, the results show that the benefits of the DBR-LDs can be obtained without a significant performance penalty in power compared to FP-LDs.

II. FABRICATION DETAILS

The semiconductor structure comprised three InGaAsP quantum wells (QWs) surrounded by 1.6 μm InGaAsP optical confinement layers and InP claddings, and was grown

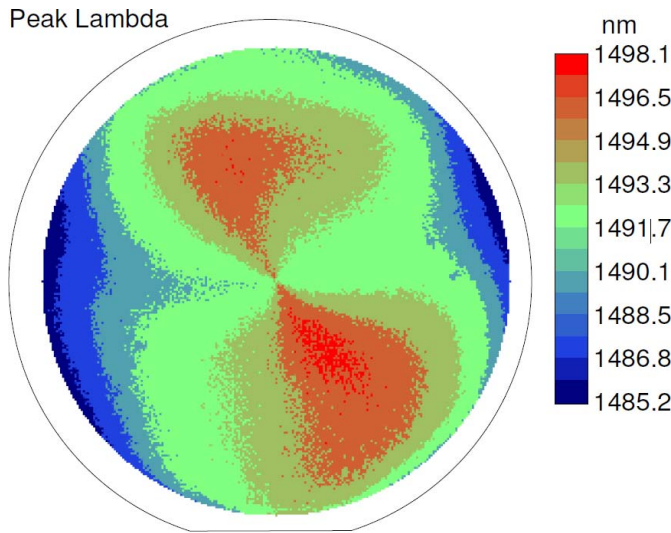


Fig. 1. Measured PL spectrum variation over the 2" wafer used in the fabrication process.

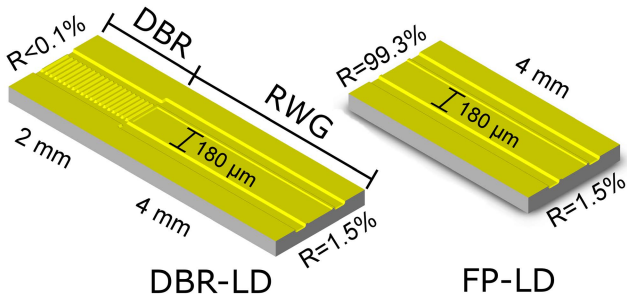


Fig. 2. Left side: drawing of the DBR-LD showing section lengths, RWG width and facet reflectivities after coating. Right side: drawing of the FP-LD showing the component length, RWG width and facet reflectivities after coating.

on 2" n-InP(100) with metalorganic vapor phase epitaxy (MOVPE). The MOVPE system produces up to 12 wafers with 2" size in a single batch and one of them was selected for the study. The QW photoluminescence (PL) correlating to FP-LD emission spectrum had a peak wavelength between 1485 nm and 1498 nm (13 nm variation) depending on the position on the substrate (see Fig. 1).

The DBR-LDs comprised two sections: a 2 mm long passive (un-pumped) third-order DBR grating section and a 4 mm long active (pumped) gain-guided ridge waveguide (RWG) section. An illustration of the component is shown on the left side in Fig. 2. A total of five different component variants were fabricated and tested with RWG and DBR widths of 180 μ m and 170 μ m, respectively, and five equally-spaced grating periods from 678.4 nm to 686.4 nm.

The DBR gratings were fabricated using soft-stamp nanoimprint lithography [10] with EVG620 mask aligner and a stamp area of 25 mm x 25 mm. The stamp was used to imprint a thin film of mr-UVCur06 photoresist (Micro resist technology GmbH) deposited on top of a SiN layer grown on the semiconductor. The photoresist was used to etch the SiN which in turn was used as a mask for etching the semiconductor. The semiconductor was etched using reactive ion etching (RIE) with CH₄/H₂ chemistry to a depth of 1010 nm from the surface

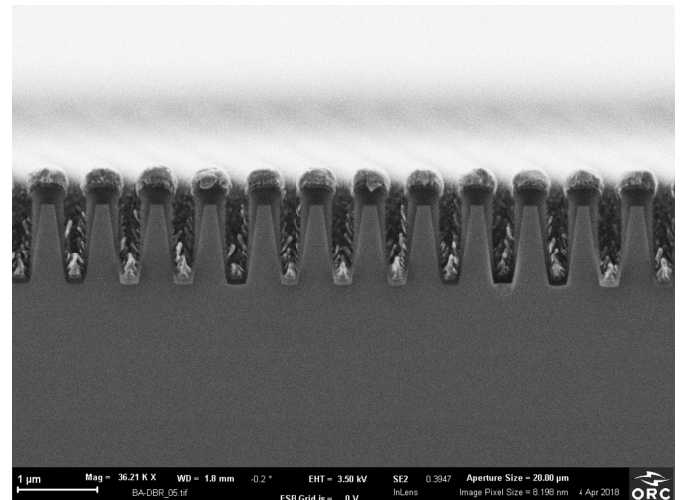


Fig. 3. Scanning electron microscope image of the grating cross-section.

of the semiconductor, 190 nm above the p-side waveguide. The etching process produced a V-shaped grating (see Fig. 3). The semiconductor filling factor was 67 % at the bottom of the grating and 24 % at the top of the grating. The walls of the grating were at an angle of 99.5°. The grating was simulated with the method outlined in [11]. This model assumes a rectangular grating with a constant filling factor, but a V-shaped grating with small sidewall angles can be approximated as a rectangular grating with a filling factor slightly smaller than at the bottom of the V-shaped grating [11]. To generate a suitable approximation, the vertically varying filling factor of the V-shaped grating was accounted for by calculating the grating parameters (coupling coefficient κ , radiative loss coefficient α_{rad}) as functions of the filling factor and then taking a weighted average in the vertical direction from the bottom of the grating to the top of the grating. The optical field intensity was used as the weighing function. This simulation yielded $\kappa = 4.8 \text{ cm}^{-1}$, $\alpha_{\text{rad}} = 4.6 \text{ cm}^{-1}$, and peak grating reflectivity $R_{\text{max}} = 0.44$.

The current confining RWG sections were fabricated using photolithography and RIE with CH₄/H₂ chemistry. They were etched to a depth of 500 nm from the surface of the semiconductor, reducing the unintentional current spreading in the heavily p-doped layers.

The injection current was limited to pass through the top of the ridge by covering the top of the wafer with SiO₂ and etching an opening on top of the ridges using photolithography and RIE. The p-side of the wafer was metallized using a Ti/Pt/Au layer stack and patterned using photolithography and a lift-off process. Finally, the wafer was thinned from n-side to a thickness of $\sim 110 \mu\text{m}$ by lapping with an AlO_x abrasive, metallized with a Ni/Au/Ge/Au layer stack, and annealed at 430 °C.

The finished wafer was cleaved into DBR-LD bars, comprising both DBR and RWG sections, and FP-LD bars, comprising only the RWG section (shown on the right side in Fig. 2). The front facets of both types of bars were coated with a single layer of Al₂O₃ with a target reflectance of 1.5 %. The back facets of the DBR-LD bars were coated with an Al₂O₃/TiO₂/Al₂O₃ stack with a target reflectance below 0.01%, and the back facets of the FP-LD bars were coated

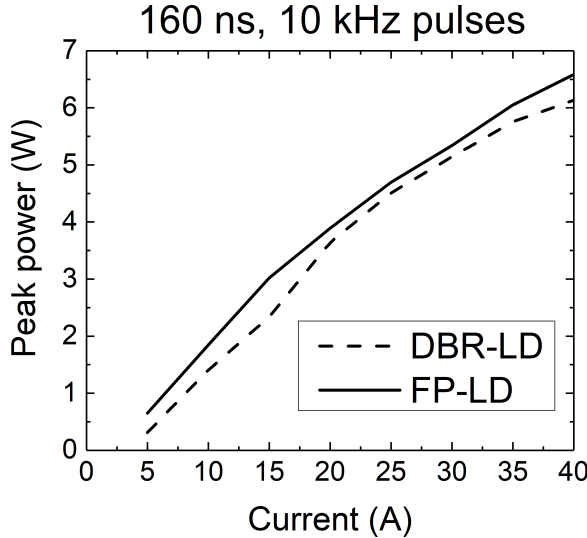


Fig. 4. The peak power of the DBR-LD and the FP-LD measured with 160 ns, 10 kHz pulses.

with eight $\text{Al}_2\text{O}_3/\text{TiO}_2$ layer pairs with a target reflectance of 99.3 %. The coatings were performed with Cutting Edge Coatings NAVIGATOR 700 ion beam sputtering system. After the coating, the bars were scribed into individual chips with a width of 400 μm . The length of the DBR-LD components was 6 mm and the length of the FP-LD components was 4 mm. Finally, the chips were mounted p-side up on metallized AlN submounts with silver epoxy glue and wire-bonded.

III. LASER PERFORMANCE

The components were characterized in pulsed operation with 160 ns, 10 kHz pulses (Dr. Heller Elektronik HLD 500-50 pulsed laser driver) and 1 μs , 10 kHz pulses (DEI Scientific PCX-7420 pulsed laser driver). The peak power of the components was measured with 160 ns current pulses with an amplitude between 0 A to 40 A. An example current-peak power (IL) curve, recorded with a Thorlabs DET08CL/M 5 GHz InGaAs photodetector and Agilent DSO9254A 2.5 GHz oscilloscope, is shown in Fig. 4. The calibration of the fast photodiode was obtained by correlating the recorded oscilloscope waveform to the average power measured with a calibrated integrating sphere. The DBR-LDs reached a peak output power of 6.1 W, while the FP-LDs reached a peak output power of 6.6 W.

The spectra of the DBR-LDs was measured up to 40 A injection current with 160 ns pulses (Yokogawa AQ6375 optical spectrum analyzer) and up to 15 A with 1 μs pulses (Anritsu MS9710C optical spectrum analyzer). The resolution in both measurement setups was 0.05 nm. A typical full width at half-maximum (FWHM) spectral width of the DBR-LDs was 0.30 nm. As a reference, the FWHM of the FP-LD was 6.9 nm at 40 A current. The spectra from a DBR-LD at various injection currents are shown in Fig. 5.

The effect of the DBR grating on the emission wavelength stability at different mount temperatures was studied by comparing the peak wavelength shift of the DBR-LD components to the peak wavelength shift of the FP-LD components. The measured spectra are shown in Fig. 6.

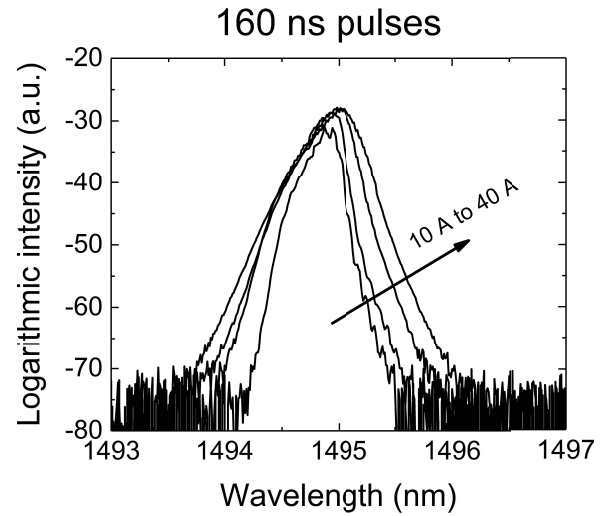


Fig. 5. Spectra from a DBR-LD with 160 ns pulses. The FWHM at 40 A injection current is 0.30 nm. The resolution is 0.05 nm.

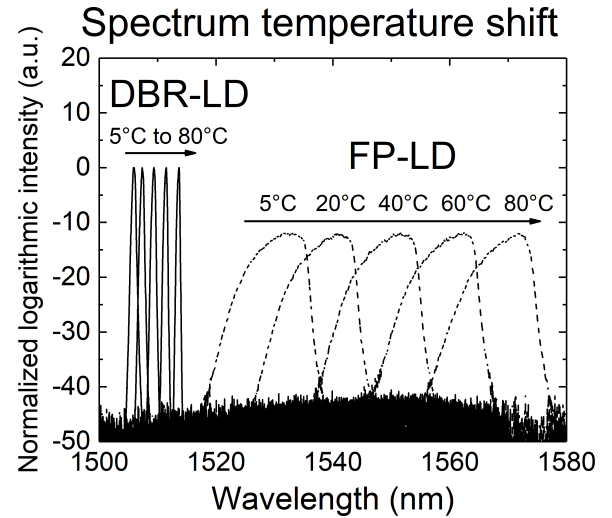


Fig. 6. The spectra of a DBR-LD chip (solid lines) and a FP-LD chip (dashed lines) at various temperatures measured in 1 μs pulsed operation. The DBR-LD peak wavelength shifts at a rate of 0.1 nm/ $^{\circ}\text{C}$ and the FP-LD peak wavelength shifts at a rate of 0.5 nm/ $^{\circ}\text{C}$.

The DBR-LDs exhibited a peak wavelength shift of 0.1 nm/ $^{\circ}\text{C}$ while the FP-LDs exhibited a peak wavelength shift of 0.5 nm/ $^{\circ}\text{C}$. This is expected, since in the DBR-LD the emission wavelength shift is dominated by the change in the refractive index of the DBR grating [12], and in the FP-LD the emission wavelength shift is caused by the change in the QW bandgap [13]. Furthermore, in the DBR-LDs, the peak wavelength was linearly dependent on the DBR grating period as shown in Fig. 7, demonstrating that the grating can be used to control the emission wavelength accurately even when the gain maximum is detuned by over 30 nm. Fig. 7 also shows the effective refractive index n_{eff} calculated from the measured emission wavelengths λ , known grating periods Λ , and known grating order l using the equation for the Bragg condition [14]

$$l \frac{2\pi}{\Lambda} = \frac{4\pi n_{\text{eff}}}{\lambda}. \quad (1)$$

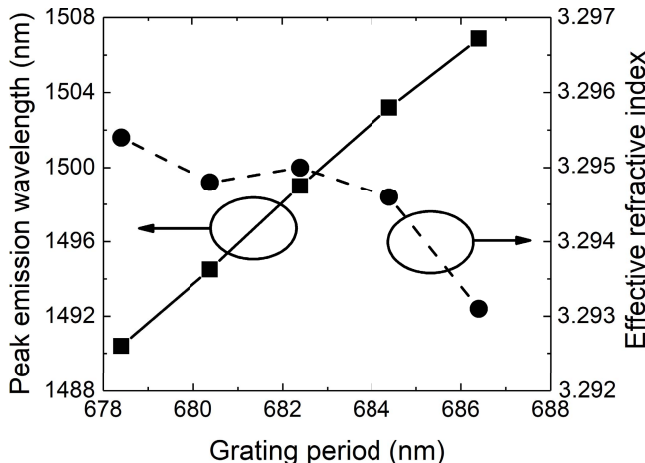


Fig. 7. The peak emission wavelength of the DBR-LD at 20 °C mount temperature and 10 A, 1 μ s pulsed injection across multiple components with different DBR grating periods and corresponding effective refractive indices. The gain maximum of the components was at 1522 nm.

IV. CONCLUSION

In conclusion, we reported high-power broad-area 1.5 μ m InGaAsP DBR laser diodes with parameters targeting eye-safe LIDAR, range-finding, and flash illumination applications. The spectral properties provided by the DBR-LDs enable the implementation of systems with low noise receivers by employing narrow pass-band filters. The DBR locks the lasing to the grating even when the detuning between the gain and the grating is over 30 nm, enabling the fabrication of large batches of LDs with identical emission characteristics and high yield. With 160 ns, 40 A injection pulses, the components exhibited a peak output power of 6.1 W and 0.30 nm spectral FWHM. The peak emission wavelength drifted by 0.1 nm/°C, which is five times less than for the FP-LD component geometry.

ACKNOWLEDGMENT

The authors wish to acknowledge the contribution of Modulight, Inc., which provided the epiwafer, and the work done by M.Sc. Mervi Koskinen in component fabrication, M.Sc. Jarno Reuna in thin film coating, and M.Sc. Heidi Tuorila in measurement setup construction.

REFERENCES

- [1] B. Schwarz, “LIDAR: Mapping the world in 3D,” *Nature Photon.*, vol. 4, no. 7, pp. 429–430, 2010.
- [2] *Safety of Laser Products—Part 1: Equipment Classification and Requirements*, document IEC 60825-1:2014, International Electrotechnical Commission, 2014.
- [3] A. Samman *et al.*, “Potential use of near, mid and far infrared laser diodes in automotive LIDAR applications,” in *Proc. 52nd Veh. Technol. Conf. (VTC)*, Boston, MA, USA, Sep. 2000, pp. 2084–2089.
- [4] O. Steinvall, R. Persson, F. Berglund, O. K. S. Gustafsson, and F. Gustafsson, “Using an eyesafe military laser range finder for atmospheric sensing,” in *Proc. SPIE Def. + Sec.*, Baltimore, MD, USA, vol. 9080, Jun. 2014, p. 90800W. [Online]. Available: <https://www.spiedigitallibrary.org/conference-proceedings-of-spie/9080/90800W/Using-an-eyesafe-military-laser-range-finder-for-atmospheric-sensing/10.1117/12.2049044.short?SSO=1>; doi: 10.1117/12.2049044.
- [5] F. Amzajerdian, D. F. Pierrottet, G. D. Hines, L. Petway, and B. W. Barnes, “Fiber-based Doppler lidar for vector velocity and altitude measurements,” in *Proc. Frontiers Opt.*, San Jose, CA, USA, Oct. 2015, Paper LTu3I.2.
- [6] A. Knigge *et al.*, “Wavelength-stabilized high-pulse-power laser diodes for automotive LiDAR,” *Phys. Status Solidi A*, vol. 215, no. 8, p. 1700439, 2018.
- [7] J. Fricke *et al.*, “High-brilliance diode lasers with monolithically-integrated surface gratings as sources for spectral beam combining,” in *Proc. High Power Diode Lasers Syst. Conf. (HPD)*, Coventry, U.K., Oct. 2013, pp. 2–3.
- [8] S. R. Selmie *et al.*, “Single frequency 1550-nm AlGaInAs-InP tapered high-power laser with a distributed Bragg reflector,” *IEEE Photon. Technol. Lett.*, vol. 14, no. 7, pp. 890–892, Jul. 2002.
- [9] A. T. Aho *et al.*, “High-power 1550 nm tapered DBR laser diodes for LIDAR applications,” in *Proc. Eur. Conf. Lasers Electro-Opt.*, Munich, Germany, 2017, Paper CB_7_4.
- [10] J. Viheriälä *et al.*, “Applications of UV-nanoimprint soft stamps in fabrication of single-frequency diode lasers,” *Microelectron. Eng.*, vol. 86, no. 3, pp. 321–324, Mar. 2009.
- [11] H. Wenzel, J. Fricke, J. Decker, P. Crump, and G. Erbert, “High-power distributed feedback lasers with surface gratings: Theory and experiment,” *IEEE J. Sel. Top. Quantum Electron.*, vol. 21, no. 6, pp. 352–358, Nov./Dec. 2015.
- [12] L. A. Coldren, S. W. Corzine, and M. L. Mašanović, “Mirrors and resonators for diode lasers,” in *Diode Lasers and Photonic Integrated Circuits*, 2nd ed. Hoboken, NJ, USA: Wiley, 2012, p. 135.
- [13] K. P. O’Donnell and X. Chen, “Temperature dependence of semiconductor band gaps,” *Appl. Phys. Lett.*, vol. 58, no. 25, pp. 2924–2926, 1991.
- [14] L. A. Coldren, S. W. Corzine, and M. L. Mašanović, “Perturbation, coupled-mode theory, modal excitations, and applications,” in *Diode Lasers and Photonic Integrated Circuits*, 2nd ed. Hoboken, NJ, USA: Wiley, 2012, p. 344.